

# Experiments in Charge Control at Geosynchronous Orbit—ATS-5 and ATS-6

R.C. Olsen

*The University of Alabama, Huntsville, Alabama*

## Introduction

**N**ONZERO spacecraft potentials have been noted since the beginning of satellite flights. Large negative potentials (hundreds to thousands of volts) were first observed on Applied Technology Satellite-5 (ATS-5) in eclipse.<sup>1</sup> These were explained as the natural result of a balance of the ambient electron and ion currents with associated secondary electron currents. In sunlight, photoemission normally provides a large enough current to preclude negative spacecraft potentials. Therefore, it was difficult to explain the negative potentials found in sunlight, first on ATS-5 and then on Applied Technology Satellite-6 (ATS-6).<sup>2,3</sup> This problem gained importance when it became clear that there was an association between spacecraft charging and anomalies in spacecraft behavior.<sup>4</sup> Further study of the daylight charging phenomena on ATS-6 showed the existence of an electrostatic barrier around the science package, and it was postulated that differential charging of insulators might be the cause.<sup>5</sup> Eventually, it was shown that the large insulated dish antenna was responsible for the barrier around the instrument package and that differential potentials of hundreds to thousands of volts existed on the spacecraft surface.<sup>6</sup>

The study of the charging process was accompanied by a program of study to determine effective methods of charge control, in particular making use of the ATS-5 and ATS-6 ion engines as current sources. In the sections which follow, the data and analysis for the ion engine experiments on ATS-5 and ATS-6 are presented, with a brief comparison to one operation of the Spacecraft Charging at High Altitudes (SCATHA) satellite (also, the P78-2 satellite) electron gun. It will be shown that electron emission from a satellite with insulating surfaces is not an effective method of charge control because the increase in differential charging that results limits the effectiveness of electron emitters and increases the possibility of electrostatic discharges between surfaces at different potentials. Plasma emission is shown to be effective because the addition of an ion source allows for the discharge of insulating surfaces as well as the spacecraft mainframe.

## Satellites and Instrumentation

### ATS-5

ATS-5 was launched into synchronous orbit on August 12, 1969, and stationed at 105° W longitude. The spacecraft, illustrated in Fig. 1, was cylindrical with an exterior dominated by solar arrays. Cavities at the top and bottom contained a mixed assortment of insulators and conductors. The fiberglass bellyband was the location of most of the instruments and experiments. These provided the majority of the conducting area on the spacecraft.

The plasma detectors were electrostatic analyzers for electrons and ions from 50 eV to 50 keV in 62 exponential steps, and had 12% energy resolution. One energy scan required approximately 20 s. One pair of detectors was aligned to the spin axis (nominally parallel to the magnetic field), with the other pair perpendicular to the spin axis and magnetic field.<sup>1</sup>

The ion engines were small cesium thrusters with filament neutralizers. The filaments, illustrated in Fig. 2, can be seen near the outer edge of the thruster. A voltage drop of a few volts across the filament provided a small range of emitted energies in the electron-volt region.

### ATS-6

ATS-6 was launched into geosynchronous orbit on May 30, 1974. The three-axis-stabilized spacecraft is illustrated in Fig. 3, with the Environment Measurements Experiment (EME) package shown at the top, the large dish antenna and solar arrays extending outward, and the Earth Viewing Module (EVM) at the focus of the antenna. The ion engine experiment was located on the EVM, with complete assemblies on the north and south faces of the EVM. The plasma detector was located on an outer corner of the EME package, and thus physically separated from the ion engine by 10 m and by the dish antenna. The mesh antenna is transparent to charged particles, however, and is a barrier to ion motion only when positively charged. It is constructed from a Dacron mesh which was copper flashed and then coated with a silicon lubri-

---

Richard Christopher Olsen received a B.S. in physics from the University of Southern California in 1974 and his Master's and Ph.D. in physics from the University of California at San Diego in 1976 and 1980, respectively. His thesis was based on the analysis of the charging phenomena observed on ATS-5 and ATS-6, particularly the results of charge control experiments on those satellites. A natural extension of this work has been the analysis of thermal plasma characteristics, and the dependence of low energy ion and electron measurements on spacecraft charging. This work led to the discovery of a normally "hidden" ion population, first with the SCATHA satellite and then with Dynamics Explorer 1. Dr. Olsen has proposed plasma sources to "ground" magnetospheric satellites, enabling experiments to measure the ambient plasma more completely and accurately. He has published articles on spacecraft charging, the effects of spacecraft charging on particle measurements, and the nature of the low energy plasmas of the inner magnetosphere. He is currently an assistant research professor in the Physics Department at the University of Alabama in Huntsville.

cant to aid in thermal control and deployment. Therefore, it is an insulator and capable of charging with respect to the mainframe.

The plasma detector was designed to measure the ambient particle population from 1 eV to 80 keV in energy, as a function of energy, time, and angle. Two detector heads rotated in orthogonal planes, and each head contained paired ion and electron detectors. An additional ion detector was fixed to the EVM/EME frame. One scan in energy requires 16 s, one rotational sweep requires 2½ min. Detector angles are defined such that 90 deg corresponds to looking radially away from the spacecraft, or straight "up."<sup>7</sup>

The thruster design is illustrated in Fig. 4. Two parallel grids are used to extract the plasma, with the outer accelerator grid at -550 V and the inner screen grid at +550 V. The 8-cm-diam thruster produced 4.5 mN thrust, with 0.1 A of cesium ions at a final kinetic energy of 550 eV.<sup>8</sup> The hollow cathode plasma bridge neutralizer is necessary to provide charge and current balance for the main beam and is an excellent plasma source when operated separately. The hollow cathode is provided with an auxiliary electrode, or probe, slightly above the cathode. In operation, cesium is fed through the cathode, and an arc is struck between the probe and cathode. The probe is initially held at 150 V with respect to the neutralizer and then drops in potential as current begins to flow.

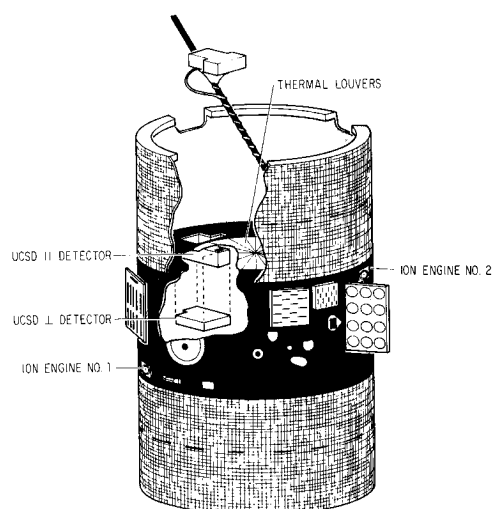


Fig. 1 ATS-5 spacecraft.

The emission characteristics of the neutralizer vary with cathode temperature and cesium flow rate. At low cathode temperatures (typically in startup), operation is in a low emission current, high extraction voltage mode named plume mode for the appearance of the discharge. Once the cathode heats up, the cesium flow rate increases and the plasma bridge enters spot mode. Spot mode is characterized by high emission currents at low extraction voltages. The neutralizer can provide substantial electron current in either mode, but does not become an efficient ion source until spot mode.

#### SCATHA

The P78-2 (SCATHA) satellite was launched into a near-geosynchronous orbit on January 30, 1979. SCATHA is a cylindrically shaped satellite, similar to ATS-5, with a 1.7-m diameter and 1.75-m length. It is spin-stabilized at a rate of about 1 rpm. It carried particle detectors similar to those used on ATS-6. In addition, it carried an electron gun to be used for charge control experiments. The electron gun provided a variety of current and voltage options, ranging from 1  $\mu$ A to 13 mA, and 50 V to 3 kV.

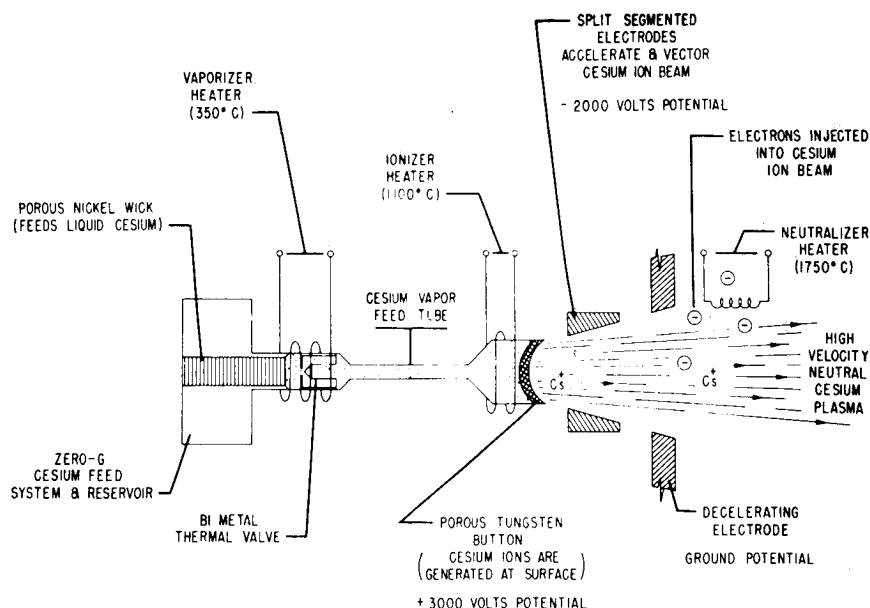
#### Thermal Electron Emission—ATS-5

In 1974 a program of operations was begun to study means of modifying spacecraft potentials. On ATS-5 the filament neutralizers on the ion engine experiment were used to emit thermal electrons in attempts to discharge ATS-5 in eclipse periods. The program had mixed results. The large potentials were usually reduced in size, but the spacecraft was rarely totally discharged in this manner.<sup>9,10</sup> Modeling of these operations was done with one-dimensional current balance models and a more sophisticated three-dimensional program. It was found that the neutralizer filament emission was limited by a potential barrier produced by differential charging on the spacecraft surface. The ATS-5 data and modeling are described below. The first sections which follow present data from the neutralizer operations, and the results from applying one-dimensional and three-dimensional models to the neutralizer operations follow.

#### Operations of the Filament Emitter

ATS-5 normally charged from -1 to -10 kV in eclipse, as determined from the ion data and the shift in particle spectra as the spacecraft moved from sunlight to eclipse. Data from ATS-6 presented similar results in 1974. Stationed at 94° W longitude, the newer satellite encountered almost the same en-

Fig. 2 ATS-5 ion engine with filament neutralizer.



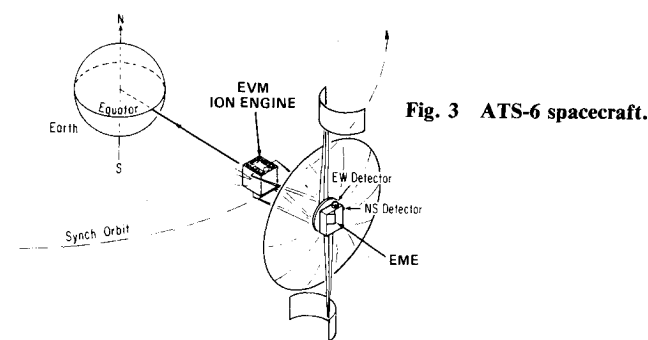


Fig. 3 ATS-6 spacecraft.

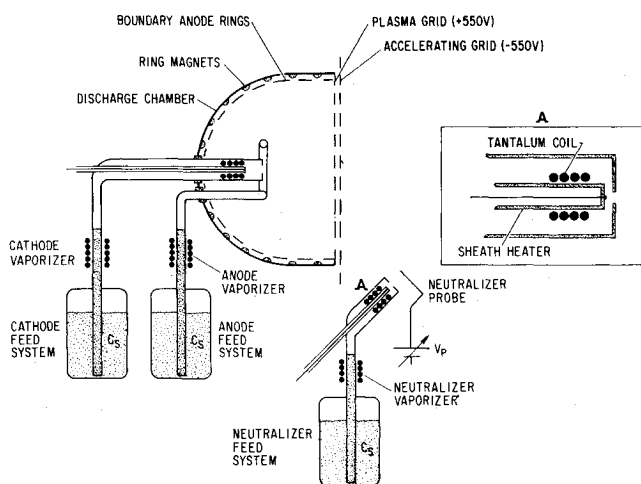


Fig. 4 ATS-6 ion engine with hollow cathode neutralizer.

vironment as ATS-5. Potential measurements made in eclipse on the two satellites were remarkably close when the environment was constant over the distance. Because of this, it was possible to use ATS-6 data as a control for comparison purposes during operations of the ATS-5 filaments.<sup>9</sup>

Data from such a neutralizer operation on September 20, 1974 are presented in Fig. 5. The ATS-6 potential varies between  $-1$  and  $-4$  kV, as does the ATS-5 eclipse potential when the neutralizer is off. The ATS-5 eclipse period ran from 06:23 to 07:30, and ATS-6 was eclipsed from 05:37 to 06:42. There is a sharp rise in potential caused by the neutralizer from 06:31:25 to 06:35:25. The potentials of the two spacecraft were determined by using the cutoff in the ion data due to the acceleration of low-energy ions up to the spacecraft potential. The values would be subject to about  $\pm 5\%$  error due to the energy window width for an ideal detector. ATS-5 responds immediately to the neutralizer "on" command, rising to near-zero potential between two data points. There is a smooth drop in the potential following the initial discharge peak. The neutralizer "off" command is followed by an immediate drop in potential to the equilibrium eclipse value.

Similar behavior is seen in most of the hundreds of operations carried out over the next two years. One outstanding question raised by the early, brief operations was: Will the spacecraft potential reach an equilibrium in a longer operation?

As longer operations were run, it was found that the charging rate slowed to near zero after several minutes. However, another time-dependent effect became apparent. In some operations, there was a short but noticeable undershoot in the potential when the neutralizer was turned off; i.e., the potential became more negative than the normal equilibrium potential would have been in eclipse.

This effect can be seen in the data from March 28, 1978 in Fig. 6. The dip visible at 04:41 is one of the most pronounced such events. Typically, the dip would only last through one or

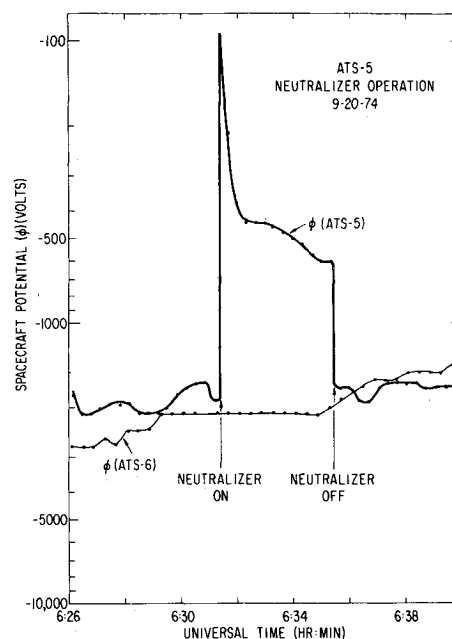


Fig. 5 ATS-5 neutralizer operation, September 20, 1974.

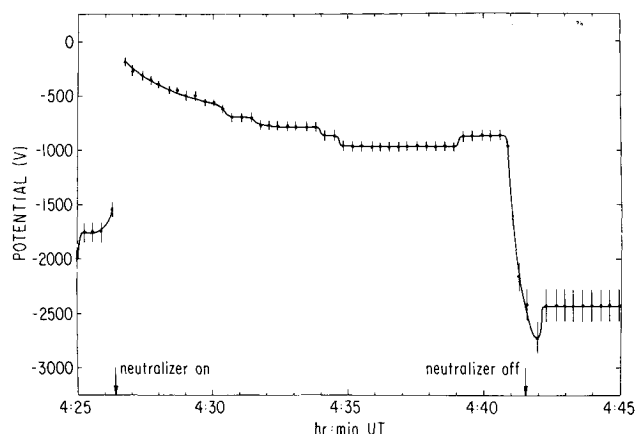


Fig. 6 ATS-5 neutralizer operation, March 28, 1978.

two energy scans, i.e., 20-40 s. At first, this dip in potential was thought to be an anomaly in the data, but repeated appearance of the phenomenon during such operations indicated it was a real effect.

Data from two of the 194 days of operations have been shown. The features commonly seen are the sharp rise in potential at the neutralizer "on" command, occasionally to above the  $-50$ -V limit of the particle data. This was followed by a rapid drop in spacecraft potential, a drop which slowed as the potential seemed to approach a new equilibrium. It was found that whenever the spacecraft had charged negatively in eclipse, operation of the filament could partially discharge the spacecraft, but the neutralizer was most effective at low or moderate potentials. Figure 7 shows the results of a comparison of the spacecraft potential with the neutralizer off with the equilibrium value with the neutralizer on for 70 cases. Most data points indicate multiple measurements at a given pair of potentials. The diagonal line shows the neutralizer "on" equals neutralizer "off" locus. Potentials for neutralizer off were taken as an average around the operation time, and potentials for neutralizer on were taken after the neutralizer had been on for 1-2 min. The neutralizer consistently causes the spacecraft to discharge, with relatively greater effects at lower equilibrium eclipse potentials.

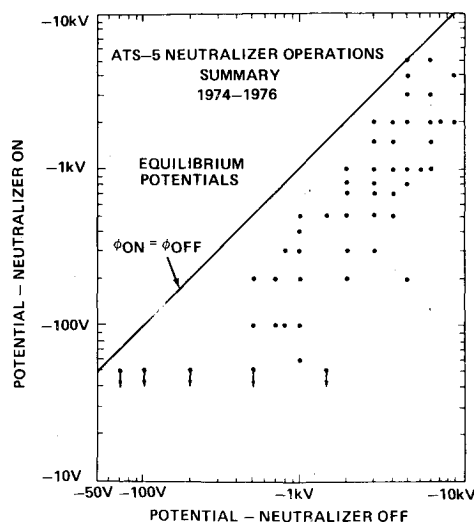


Fig. 7 ATS-5 neutralizer operations summary.

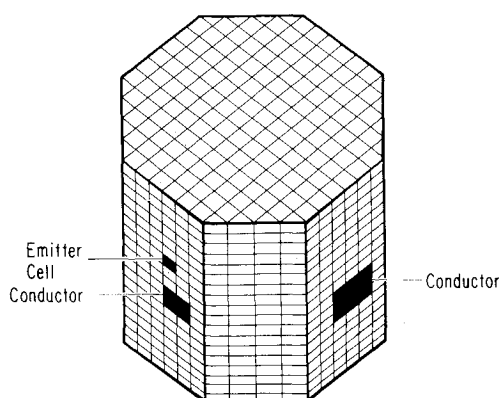


Fig. 8 ATS-5 NASCAP model.

### Charging Models

The objective of the analysis of these events was to determine the currents necessary to discharge the satellite. This required the development of a model for the equilibrium current balance to the spacecraft, in order to estimate the portions of the current balance that could not be measured directly. Once it became clear that there were time dependences in the data, a second goal was to understand the physical processes causing these variations. The first model to be developed is an extension of the one-dimensional current balance model originally used to explain the ATS-5 charging behavior.<sup>1</sup> This model is an equilibrium model and does not attempt to describe time-dependent changes. These later effects were studied with the NASA Charging Analyzer Program (NASCAP), a three-dimensional, time-dependent, charging analysis program.

### One-Dimensional Current Balance Model

A one-dimensional current balance model was developed to model the equilibrium currents to the spacecraft. This was done to estimate the current emitted by the hot filament. The work followed the patterns established by earlier workers.<sup>1,11</sup> The plasma detectors measure the ambient fluxes which reach the spacecraft. These fluxes can then be used to calculate the secondary electron fluxes from the spacecraft. Since the net current to the spacecraft should be zero in equilibrium, the use of an artificial source of particles will create an imbalance in the net flux to the spacecraft.

The plasma detectors provided the 50-eV to 50-keV particle flux data for the current measurement. In the environments studied, this energy range provides the bulk of the current to

Table 1 ATS-5 neutralizer emission results

Date	Time	Equilibrium potential kV	Maximum current density, pA/cm <sup>2</sup>	Equilibrium current density, pA/cm <sup>2</sup>
9-19-74	07:15	-6.0	45	10
9-20-74	06:33	-2.0	60	30
9-30-74	06:36	-2.7	45	30
9-30-74	07:15	-1.9	60	20
10-1-74	06:35	-1.0	30	20
10-2-74	06:36	-7.0	35	25 <sup>a</sup>
10-4-74	06:40	-0.1	-15	-10
10-7-74	06:45	-1.1	25	10
10-7-74	06:56	-0.6	15	10

<sup>a</sup>Spacecraft may have gone positive during emitter operation.

the spacecraft from the ambient plasma. It was assumed that the environment was isotropic, since the data quality and model could not support an analysis including pitch angle anisotropy.

Secondary electron yields have been modeled as a function of the energy and angle of incidence for a great variety of materials. Since the spacecraft materials were not characterized before launch, material parameters for aluminum were used. These values would not be greatly different from those for the oxide coating on the solar arrays. The initial values for the true secondary yield for aluminum were a peak of 1 at 400 eV.<sup>1,11,12</sup>

The use of aluminum parameters for secondary yield required a calibration of the model to obtain more accurate numbers for the secondary yield. Data from 1969 and 1970 were used in the manner described by DeForest.<sup>1</sup> A slightly more extensive data set was used with essentially the same results. The error measurement for the calibration was the net flux divided by the ambient electron flux. An rms error of 12% was found at the final calibration.

The current balance model was applied to the ATS-5 electron emitter operations, with results shown in Table 1. The net fluxes are now a measure of the current emitted by the hot filament. Conversion from flux to current requires integration of the flux over the area of the spacecraft. The question of which surface area to use becomes apparent at this time. The current balance the neutralizer is involved in is the balance to the mainframe of the spacecraft. Therefore, the conducting area of the spacecraft is the area to use in the integration. The cylindrical spacecraft has the following dimensions: length = 184 cm, diameter = 146 cm, for an area of 12 m<sup>2</sup>, neglecting the interior walls of the cavities. The conducting area is not accurately known, but is about one-tenth of the total area. The results of the ATS-5 modeling program for nine cases are reported in the form of current densities. The maximum current density is the value obtained at the maximum (least-negative) potential. The equilibrium value is obtained 1 or 2 min into the operation, after the rapid changes in potential have ceased. The equilibrium potential is the spacecraft potential before the emitter is used.

Net fluxes of 30 pA/cm<sup>2</sup> were obtained from the equilibrium data, with maximum values at 60 pA/cm<sup>2</sup> obtained at the discharge peak. This gives an equilibrium current of 0.3  $\mu$ A assuming a conducting area of 1 m<sup>2</sup>. The equilibrium current of 0.3  $\mu$ A was substantially below the capabilities of the emitter (nominally milliamps). This fact, coupled with the peculiar time dependence of the potentials, lead to a consideration of how the current might be limited.

Space-charge effects were considered, but could not explain the observed time dependences. Most reasonable space-charging-limiting processes would occur much more rapidly than the effects seen on ATS-5.

The solution was found to involve differential charging of the spacecraft surfaces. Because the majority of the spacecraft

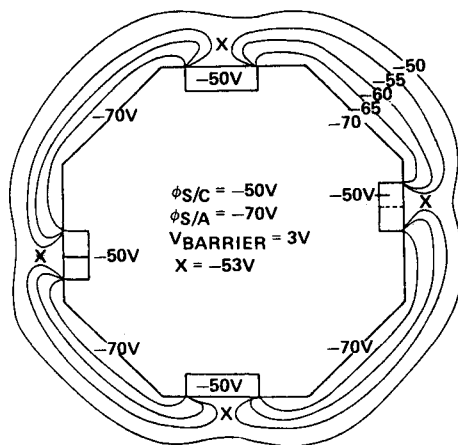


Fig. 9 ATS-5/NASCAP potential contours.

Table 2 ATS-5 object material properties

Property	Aluminum	SiO <sub>2</sub>
Dielectric constant	1	4
Thickness, m	$1 \times 10^{-3}$	$2.75 \times 10^{-4}$
Bulk conductivity, mho/m	—	$2.75 \times 10^{-12}$
Atomic number	13	13
Maximum secondary yield	2.4	2.4
Energy for maximum yield, keV	0.35	0.35
Backscatter-range parameters <sup>a</sup>		
P7	260	260
P8	1.3	1.3
P9	240	240
P10	1.73	1.73
Yield for 1-keV ions	0.7	0.7
Ion energy for maximum yield, keV	40	40
Photoelectron yield in sun, A/m <sup>2</sup>	0 <sup>b</sup>	0 <sup>b</sup>
Surface resistivity	—	—

<sup>a</sup>Range (Å) =  $P7E^{P8} + P9E^{P10}$ ,  $E$  in keV. <sup>b</sup>No photoemission except from emitter spot.

surface is insulating, it is able to hold a potential substantially different from the spacecraft mainframe. It will be shown subsequently that such potentials can limit the neutralizer current. Finally, because of the difference in magnitudes of the spacecraft to plasma capacitance ( $\sim 10^{-10}$  F) and solar array to mainframe capacitance ( $\sim 10^{-6}$  F), the two time constants observed in the data are explainable as the time constants of the two capacitances. This will be seen in the time-dependent model below.

### Three-Dimensional, Time-Dependent Modeling

The twin problems of a limiting process and time dependence require a code which can calculate fluxes to a three-dimensional object, and do so for the time-dependent case of switching on and off an artificial current. A three-dimensional analysis is required to obtain the electrostatic barrier generated by an uneven distribution of surface potentials.

The NASCAP program was developed for the solution of equilibrium and time dynamic charging problems in a magnetospheric environment.<sup>12,13</sup> Objects are modeled on a  $16 \times 16 \times 33$  grid with up to 15 different materials. The internal capacitances of the spacecraft are defined and calculated, as well as the capacitance of the spacecraft to the distant plasma. Space-charge effects are left out, and Laplace's equation is used to determine the potentials in space around the object. Given an initial potential distribution on the spacecraft, the fluxes to the spacecraft are calculated based on a specific environment. A one-dimensional (spherical) approximation is

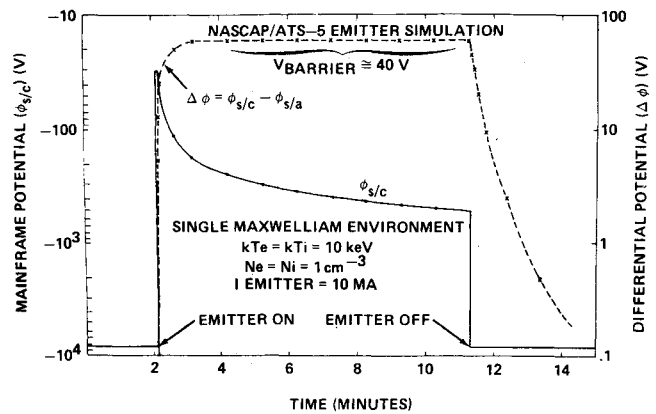


Fig. 10 ATS-5/NASCAP emitter simulation.

used to calculate the flux to each surface. Secondary fluxes emitted from those surfaces are calculated based on the ambient fluxes. The effects of local electric fields on those emitted currents, i.e., barrier effects, are included, and can limit the emitted secondary electron flux. Barrier effects are also checked in the photoemission flux calculation. The code then iterates, calculating the change in potentials and field caused by the current flow, then the new currents in the new electric field distribution. The accuracy of the code is largely a question of how accurately the material properties are known.

The ATS-5 satellite was modeled as shown in Fig. 8, filling most of the first grid. The object is embedded in a larger grid twice the size of the inner grid. In the ATS-5 object shown in Fig. 8, small conducting areas (dark) are surrounded by insulators (light).

The secondary emission properties of all surfaces are those of aluminum, a concession to a lack of knowledge of ATS-5 surface properties. The insulators and conductors differed only in their resistivity in the model object. Parameters are given in Table 2.

In the initial computer runs, potential distributions were established on the spacecraft to study the resulting fields. The objective was to establish an electrostatic barrier to electron emission. It was found that almost any nonuniform potential distribution did so! Figure 9 shows the results for a spacecraft at  $-50$  V, with insulators at  $-70$  V. The potential contours are given in the plane perpendicular to the spacecraft axis, midway along the axis. These conditions generated a saddle point at  $-53$  V in front of the conducting surfaces, which results in a barrier of 3V to electrons. Electrons emitted from the conducting spacecraft surfaces with less than 3 eV kinetic energy will be returned to the surface. This demonstrated that differential charging of the spacecraft could quickly lead to a limitation of the current emitted by the hot filament.

The final stage of the modeling was to attempt to duplicate the time dependence of the data. The electron emitter was modeled as a  $10\text{-}\mu\text{A}$  source of photoelectrons, which the computer object emits with a thermal energy of 2 eV. Surfaces were given the secondary emission properties of aluminum. The model spacecraft had a capacitance to the distant plasma of 104 pF, and a much larger capacitance to the solar array of  $1.3\text{ }\mu\text{F}$ . Thus the capacitance governing differential charging was 10,000 times larger than the capacitance corresponding to the mainframe to plasma potential difference. Given that the net current to the spacecraft at any time is roughly proportional to the potential of the spacecraft, an effective resistance can be invoked. When combined with the system capacitance, this gives an effective time constant for the time-dependent effects seen. The large difference in capacitances implies the time constants for charging and differential charging will show a substantial difference.

The results for a 10-keV Maxwellian environment are shown in Fig. 10. The solid line (with dots) shows the mainframe

potential, with a scale to the left. The dashed line shows the differential potential, with a scale on the right axis. The noteworthy points here are not the magnitudes of the voltages, but rather the relative shapes of the curves. At time zero, the spacecraft is allowed to charge negatively to equilibrium. At 2 min, the emitter is started. The spacecraft potential drops promptly (milliseconds). Until this time, no differential potentials had developed. The solar array now begins to charge negatively again, limited by the capacitance of the solar arrays to the spacecraft mainframe. Within 10 s, the solar array is 20 V negative with respect to the spacecraft and a barrier is forming. Once a barrier has formed, the spacecraft potential drops back in the direction of its equilibrium eclipse value. The differential potential and barrier height stabilize, and the drop in potential slows. At emitter off, the potential promptly drops to the equilibrium value it had prior to the operation. This time development is identical to that seen in the actual operations. Different environments gave slightly different potentials, but the same time dependence and curve shapes were found.

The analysis shows that the differential charging initially develops on a time scale (seconds) faster than can be resolved with the plasma data. The gradual variations in potential seen in the data correspond to a time period when the differential potential and resulting barrier are nearly constant. The initial charging spike and development of differential charging are the results of the substantial positive current being emitted by the object. Once the barrier forms, the large positive current is greatly reduced, the object receives a much smaller net negative current, and the potential varies on a much slower time scale (tens of seconds), which is observed.

The negative overshoot at emitter off was seen in a few of the model runs, but was not always found, apparently depending upon the environment. The overshoot can be understood as part of this model. At the time the neutralizer is switched off, there is a differential potential on the spacecraft generating a barrier to low-energy electrons. There is no fundamental difference between the filament electrons and those generated by true secondary emission. If the environment is such that the true secondaries are an important part of the current balance, a barrier around the conductors will seriously affect the current balance to the spacecraft even after the emitter is switched off. It can be seen in the figure that, for this case, the differential potential has a decay time constant of about 1 min. This time constant depends on the interspacecraft capacitances, which are poorly determined. More accurate knowledge of the spacecraft structure, used in the right environment, should yield quantitative as well as qualitative agreement with actual operations.

#### Laboratory Simulation

The current limiting effects of differential charging have been studied in the laboratory using a flight spare ATS-5 ion thruster. It was found that in a chamber test up to  $4.25 \mu\text{A}$  were emitted from the filament. A model of the emitter interaction with the spacecraft surface was established by mounting the emitter in a hole in a metal plate electrically isolated from the emitter. It was found that biasing the metal plate 5 V negative with respect to the emitter lowered the emitter current to  $1 \mu\text{A}$ , duplicating the current limiting effects inferred for the space operations.<sup>14</sup> (The editor notes that this is a triode!)

#### SCATHA Electron Gun Operations

The experience obtained with the ATS-5 data and modeling are directly applicable to the data obtained from the electron gun experiments on the SCATHA satellite. The SCATHA satellite geometry was similar to ATS-5, i.e., cylindrical, and dominated by insulating surfaces. The electron emitter was considerably more sophisticated, however. The electron gun was provided with several current settings, and acceleration

voltages, designed with the idea of "punching through" the spacecraft sheath.

Some of the data from operations of the electron gun bear a remarkable similarity to the ATS-5 electron emission results. Figure 11 shows the results from a sequence of operations on April 24, 1979 (day 114). This sequence takes place during an eclipse charging event which features the largest (most negative) charging event of 1979 for SCATHA,  $-8 \text{ kV}$ , just prior to the beginning of operations. The data for this time period have been studied from the viewpoint of establishing the spectra as a "worst-case" charging environment.<sup>15</sup>

The gun current and voltage settings are indicated in the top portion of Fig. 11, with the spacecraft potential as obtained from the University of California at San Diego (UCSD) particle detectors plotted below. The spacecraft potential response bears a startling similarity to that seen on ATS-5, particularly the sequence from 07:37 to 07:38 and the one following from 07:39 to 07:40. In the former case, a potential measurement was within the same second that the voltage change command was given, and the rise in spacecraft potential was caught at  $-3.5 \text{ kV}$ . This portion of the sequence used  $100 \mu\text{A}$  and a 50 V accelerating potential, and raised the spacecraft to an equilibrium potential of  $-3 \text{ kV}$ . The following sequence at  $100 \mu\text{A}$  and 150 V may have temporarily (for a few seconds) raised the spacecraft to 0V potential, but the spacecraft quickly fell back to  $-1.5 \text{ kV}$ . (The 1-mA, 50-V operation that follows was unique because the gun was internally current limiting at a few hundred microamps.) The spacecraft is not discharged any further by increasing the current and voltage. At 07:44 the voltage and current were lowered and the spacecraft potential appears to have overshoot, as was witnessed in some of the ATS-5 operations when the neutralizer was turned off.

This operation sequence indicates that the differential potentials will develop on the spacecraft surface with magnitudes sufficient to current limit a 150 V electron gun. These operations confirm the need to provide a means of discharging the dielectric surfaces, since increasing the electron gun accelerating voltage will only increase the magnitude of the differential potentials on the spacecraft surface.

#### ATS-5 Ion Emission Experiments—Induced Charging

The converse of the discharge events described above were the active attempts to artificially raise the ATS-5 potential by emitting an unneutralized ion beam. It was originally intended

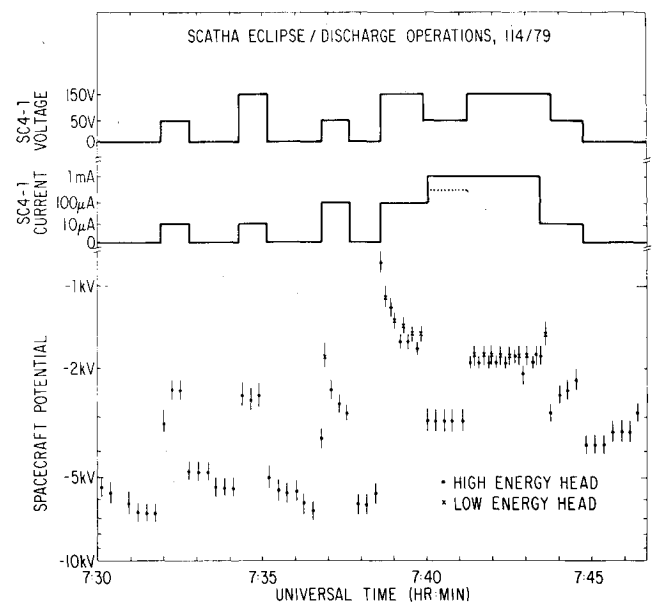


Fig. 11 SCATHA electron gun operation.

that the ATS-5 spacecraft be gravity-gradient-stabilized. However, because of a faulty orbit injection ATS-5 spun up to 100 rpm. This produced centrifugal forces so high that it was impossible to control the flow of propellant to the ion thruster in the normal manner. The result was that the thruster could be operated only for very short periods (approximately a few minutes) on a short duty cycle. In addition, because of the thruster control logic, non-neutralized operation could be obtained only during the cooling down of the ionizer. During this period no thruster telemetry was available. Only two short periods of simultaneous accelerator and particle data have been taken. The first was on July 20, 1972, during the initial testing of the accelerator. Several normal turn-ons were recorded as well as one good example of non-neutralized operation.

During the neutral beam emission experiments (ion engine mode), the magnitude of the spacecraft potential remained below 50 V in agreement with laboratory measurements of neutralizer-beam coupling potentials. With the neutralizer switch off, a different result was obtained. Figure 12 shows two ion counting rate scans from the ion detector parallel to the spin axis, for engine on and off. The spacecraft is uncharged ( $|\phi| < 50$  V where  $\phi$  is the satellite potential) when the

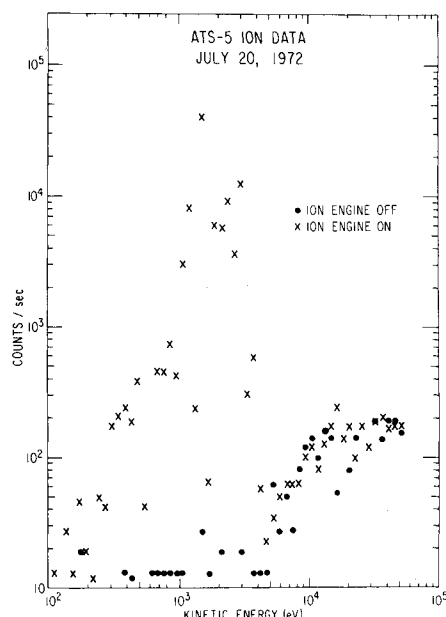


Fig. 12 ATS-5 ion emission operation.

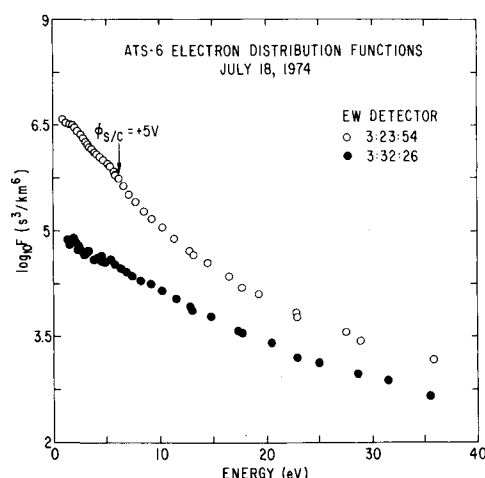


Fig. 13 ATS-6 electron distribution functions, July 18, 1974.

engine is off, which is normal for the early afternoon environment of the spacecraft [2130 universal time (UT); ~1530 local time (LT)]. When the beam is switched on, there is a substantial increase in the ion count rate below 3 keV, particularly from 1-3 keV. The initial beam current is 160  $\mu$ A. The observed increase of low-energy positive particles with the engines on could be environmental ions that have been accelerated by the spacecraft potential, or they could be cesium ions from the ion thruster that have returned to the spacecraft. In either case, the spacecraft must be charged to a significant negative potential on the order of the beam energy (3 kV).

The initial beam ion current of 160  $\mu$ A is comparable to the integrated photoelectron current leaving the spacecraft, therefore, it is unnecessary for the beam to return to obtain a net current balance. The spread of ion counts over a range of energies during this event is probably at least partially due to fluctuations in the ion emission due to intermittent operation. As a result the spacecraft potential is probably also varying rapidly during the event.

### ATS-6 Plasma Emission Experiments

ATS-6 carried twin cesium thrusters designed to test ion engine technology and their usefulness for stationkeeping on the three-axis-stabilized satellite. They performed successfully, demonstrating thrust, an absence of interference with spacecraft systems, and beneficial effects on spacecraft potentials. In addition, the plasma bridge neutralizers were operated successfully in special operations in 1976 and 1977 to observe the changes in spacecraft potentials caused by plasma emission, complementing the ATS-5 experiments begun in 1974.<sup>16</sup>

In the sections which follow, the results of engine operations in quiet and energetic environments are presented for operations in sunlight. These are followed by a concluding example of the effect of plasma emission on a negatively charged satellite in eclipse.

#### Ion Engine 2, Thruster Operation

The first ion engine operation was on July 18, 1974. This data set shows the effects of plasma emission on a spacecraft that is initially positively charged. The data taken on this day are unique for a number of reasons besides the ion engine operation. The satellite is in the Earth's midnight region, normally an environment of hot (keV) plasmas. Because the magnetosphere had been quiet for an extended time period, the environment was an unusually cool, dense plasma and the satellite was charged a few volts positive.

The particle distribution functions prior to and during the operation provide some details of the ion engine effects. The distribution function, or phase space density, describes the particle distribution as a function of position and velocity with units of inverse volume times inverse velocity cubed. Familiar quantities such as density can be obtained by integrating the observed distribution function over all velocities or, in our case, the observed energy range. The slope of the distribution function is generally the plasma temperature, if the distribution is at or near thermal equilibrium, i.e., a Maxwellian distribution. If plasmas from two distinct sources are observed, particle data often reveal curves with different slopes and amplitudes over adjacent energy ranges. Figures 13 and 14 show the electron and ion distribution functions for 03:24 (engine off) and 03:32 (engine on) from the east-west detector. In the log-linear scale used here, a Maxwellian distribution will be a straight line. The electron data at 03:24 show a break at 5 eV, suggesting a boundary between spacecraft-generated electrons (photoelectrons) and the ambient population and, thus, a +5 V potential. The electrons below the break are characterized by a temperature of 2.45 eV and a density of 27.8  $\text{cm}^{-3}$  as determined by a least-squares fit of the 2.0- to 5.0-eV data. The ambient population has a temperature of 5 eV at low energies and a density of 2-3  $\text{cm}^{-3}$  depending on the spacecraft potential assumed in the calculation.

The ion data at 03:32 show a sharp drop at 4 eV, giving a  $-4$  V potential when the engine is on. A shift of 8 or 9 eV in the particle spectra in the appropriate directions bring them into agreement, showing that there has been an 8- or 9-V shift in the spacecraft potential.

The data were examined in this fashion throughout the operation period; the resulting potentials are shown in Fig. 15. The neutralizer probe voltage gives the status of the small plasma bridge, particularly denoting the beginning of spot mode operation. The beam current gives the status of the main thruster. The potential measurements at the bottom are subject to  $\pm 1$  V uncertainties, with error bars left off to avoid clutter. Small fluctuations in potential are probably real.

The neutralizer operation resulted in a  $-1$  V potential, while the full beam set the spacecraft to  $-4$  V. The shift to negative potentials implies a distinct change in the spacecraft

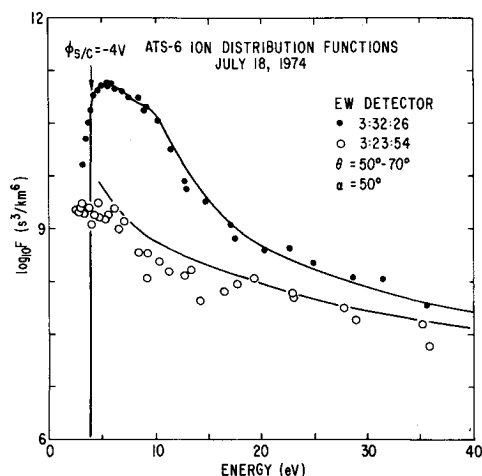


Fig. 14 ATS-6 ion distribution functions, July 18, 1974.

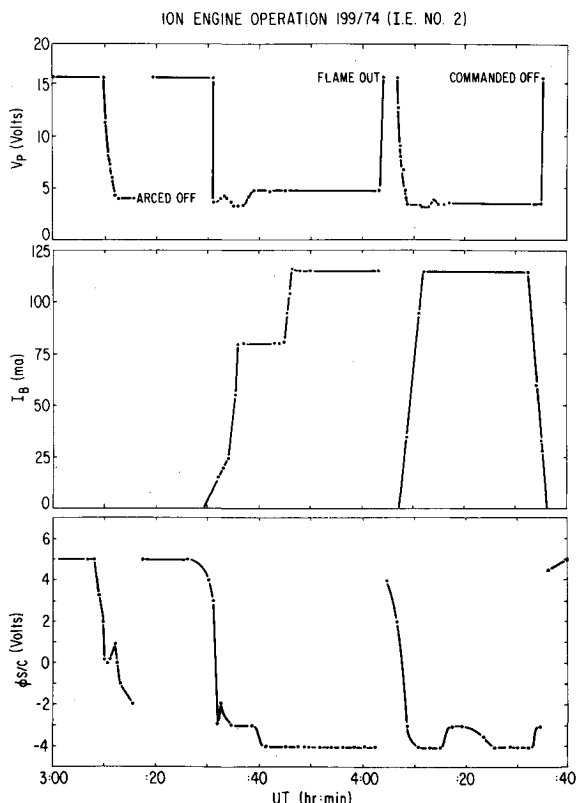


Fig. 15 ATS-6 ion engine operation, July 18, 1974.

current balance. More photoelectrons and secondary electrons will now escape, increasing the (inward) positive current to the spacecraft. The change in potential reduces the ambient electron flux and increases the ambient ion flux, again increasing the positive current to the spacecraft. These changes are balanced by a net ion current leaving the spacecraft through the beam. The small change in potential will primarily affect the thermal fluxes. The thermal electron flux has a 5-eV temperature and a density of  $2 \text{ cm}^{-3}$ , while the ion population is mostly a 1-eV  $2 \text{ cm}^{-3}$  hydrogen plasma. The secondary electron fluxes in this environment are a small percentage of the current balance. The photoelectron flux has a maximum value of  $1 \times 10^{10} \text{ cm}^{-2} \text{ s}^{-1}$ . This is reduced by a factor of 100 by the  $+5$  V potential when the neutralizer is off.<sup>17</sup> The thermal fluxes for zero potential are about  $1 \times 10^8 \text{ cm}^{-2} \text{ s}^{-1}$  for the electrons and  $8 \times 10^5 \text{ cm}^{-2} \text{ s}^{-1}$  for the ions. The balance of current gives a net ion flux from the neutralizer that basically equals the integrated photoelectron flux, about 1.6 mA assuming a  $100 \text{ m}^2$  surface area (an extreme upper bound). The ion engine telemetry gives an upper bound of 3-5 mA on the net current emitted.

No signs of cesium ions being returned to the spacecraft were found.

#### Ion Engine 1, Thruster Operation

The second successful ion engine operation began on October 19, 1974 and ran for 92 h. The environmental conditions at this time were considerably different from those found in the first test. The operation began in the midst of a substorm 2 h after local midnight. This is a disturbed environment with negative spacecraft potentials and differential charging effects visible before the operation begins. Data are available only from the north-south detector head.

An injection event at 07:05 caused the spacecraft to charge to between  $-40$  and  $-50$  V and caused an increase in the height of the differential charging barrier to about 100 V by 07:15.<sup>6</sup> The ion engine operation began at 07:40 UT. The spacecraft potential and differential charging barrier heights are given in Figs. 16 and 17. The spacecraft potential was measured by finding the lowest energy ion channel with measurable counts and taking that as the spacecraft potential. This can lead to potential measurements which are too negative if there are too few ambient low-energy ions to measure. Data points were taken with the detector at 90 deg (straight up, away from the spacecraft) to minimize the effects of local fields. The measurement assumes that the observed ions are not generated on the spacecraft, which proved to be a good assumption at this angle. The barrier height was measured by examining the electron distribution function, and finding the break or drop where the transition from spacecraft-generated particles to ambient particles occurs. These measurements were also made at 90 deg. Both measurements are subject to about 10% error due to the width of the energy channels.

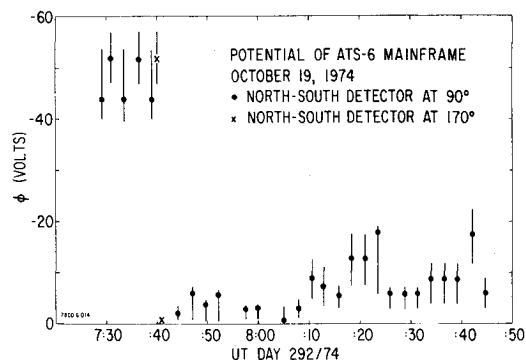


Fig. 16 ATS-6 ion engine operation, October 19, 1974.



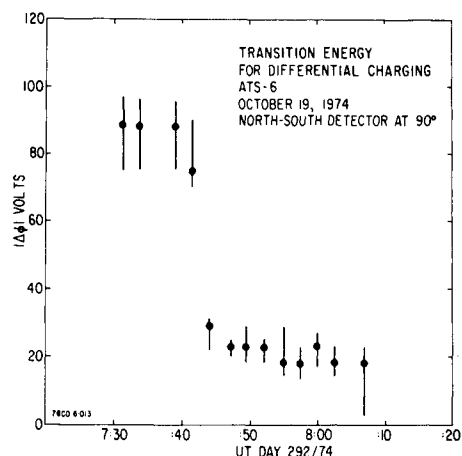


Fig. 17 ATS-6 ion engine operation, October 19, 1974.

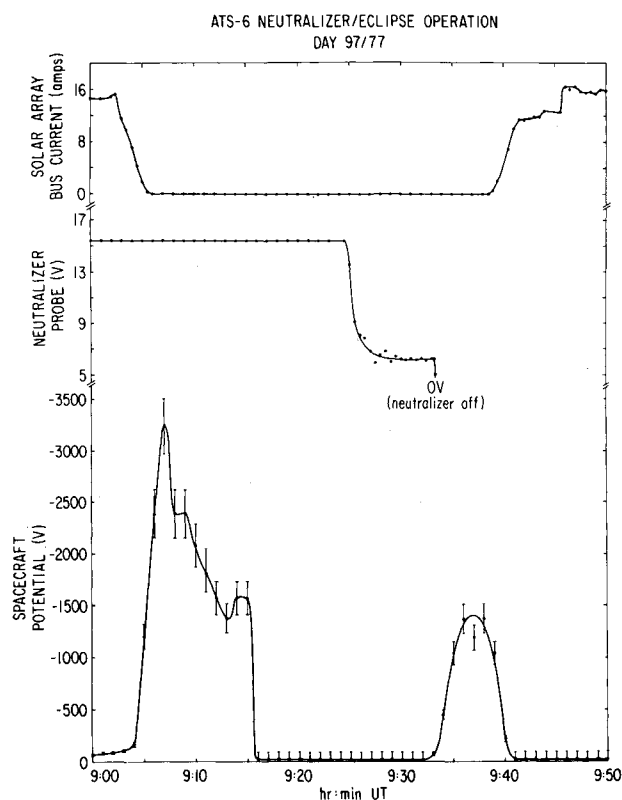


Fig. 18 ATS-6 neutralizer operation, April 7, 1977.

The plasma bridge enters spot mode at 07:41 and the spacecraft potential rises to about  $-3$  V. (The detector was at  $170^\circ$  deg at this time, therefore two data points at that position are included in the plot.) The differential charging barrier falls to about 20 V from 100 V about 2 min later. The engine ignition at 08:00 causes a slight drop in potential, and then the disappearance of the differential charging barrier. The time dependence of the observed effects helps explain the physical phenomena that are occurring.

There is an additional piece of information available in the low-energy ion observations (not shown here). The angular distribution of low-energy ions (0-20 eV) is not aligned with the magnetic field, as is normally found in this region of space.<sup>18</sup> Instead, the incident angle of the peak flux of low-energy ions varies over the period between the ignition of the neutralizer and the ion engine. Once the ion engine ignites, the incident angle of the intense low-energy ion fluxes stabilizes. These ions must be from the hollow cathode and ion engine.<sup>14</sup>

The change in the incidence angle of the intense fluxes reflects the changes in the local electric fields as the ion fluxes from the engine discharge the negative dielectrics on the top of the EVM, the antenna, and the solar arrays. In equilibrium the incidence direction stabilizes at one end of the detector rotational pattern, with particles entering tangentially along the antenna and solar array strut.

The variations in spacecraft potential with time and the identification of low-energy ion fluxes from the engine provide the information necessary to describe the sequence of changes in the electrostatic configuration of the spacecraft. Initially, the sunlit spacecraft has a number of dielectric surfaces around the conducting spacecraft components which are negatively charged with respect to the spacecraft. This condition has been shown to be the normal response of the spacecraft to an energetic particle environment. The large dish antenna has been shown to be largely responsible for the barrier around the EME module.<sup>6</sup>

The insulators on the EVM (primarily the Kapton surface of the thermal blanket) serve a similar purpose there. These barriers are essential for the development of negative potentials in this environment. Emission of electrons only (at energies below the barrier height) will not discharge the satellite. For the spacecraft to be discharged, the differentially charged insulators must be brought close to the mainframe potential. Once the barrier has been removed, an electron current from the neutralizer can escape and discharge the mainframe. Laboratory tests on hollow cathode devices show that the ion current extracted from a cathode depends on the extraction voltage and suggests that for potentials of tens of volts over distances of 10-20 cm currents of tens of microamps can be extracted.<sup>19</sup>

The apparent sequence of events is as follows:

- 1) The negatively charged spacecraft has insulating surfaces which are negatively charged with respect to the mainframe.
- 2) The neutralizer ignition into plume mode has no measurable effect on the spacecraft because the thermal electrons cannot escape through the barrier around the EVM.
- 3) Spot mode operation of the neutralizer provides an ion source capable of discharging the EVM insulating surfaces which were limiting the emission of photoelectrons and secondary electrons from the conducting surfaces of the EVM. This alone may be sufficient to allow the satellite to discharge.
- 4) The neutralizer provides an electron current as necessary to raise the spacecraft potential to  $-1$  to  $-3$  V.
- 5) Ion fluxes from the neutralizer partially discharge the antenna, but do not compete the process. The extraction field is apparently not high enough to draw sufficient current.
- 6) The engine ignites, causing a shift in the operating mode of the neutralizer and providing a large flux of charge exchange ions. These ions complete the discharge of the dielectrics, leaving only sufficient potentials to maintain the ion flux to the dielectric surfaces.

#### Neutralizer Operations in Eclipse

As part of the program to study the effects of the ion engine on spacecraft potentials and to study means of modifying potentials, the ion engine neutralizers were operated during periods of spacecraft eclipse. ATS-6 was normally at a positive potential in sunlight in quiet environments. If the positive spacecraft then entered eclipse, the particle data usually showed a small shift in the negative direction as the photoelectric current was cut off. The equilibrium potential in such eclipses was generally between  $+5$  and  $-1$  V. In energetic environments, the sunlit satellite was generally tens of volts negative to as much as 1 kV negative. Under such conditions, an eclipsed satellite normally charged to several kilovolts negative.

Analysis of the neutralizer operations associated with the full thruster tests suggests that the neutralizer should do as thorough a job of controlling the spacecraft potential in

eclipse as it did in sunlight. When operated at quiet times in eclipse (no large negative potentials) a small ion current from the neutralizer caused a shift of a few volts in the negative direction. In more active environments, larger charges were seen.

Two operations in April 1977 showed that if the spacecraft was charged several kilovolts negative, the neutralizer would discharge the satellite. Figure 18 shows the results from April 7, 1977. The solar array current reflects the illumination of the spacecraft, the neutralizer probe voltage shows its status, and the potential at the bottom comes from ion data. The spacecraft charges to  $-3$  kV in eclipse from 09:05 to 09:15, and the potential rises to near zero at 09:15 when the neutralizer ignites. The neutralizer is an excellent electron source even in plume mode, and the absence of differential charging in this case means that ions are not needed in such abundance. The spacecraft remains near zero potential until the neutralizer is switched off at 09:33. At this time, the spacecraft potential falls to  $-1.5$  kV for the few minutes remaining in eclipse. Neutralizer operation has provided the necessary electron current to discharge the satellite and maintain it at low potentials. This is in contrast to the observed results of filament emission of electrons on ATS-5. Those experiments showed that the ability of the filament emitter to discharge the satellite was extremely limited and that it could not hold the spacecraft at low potentials. The difference is the presence of ions in the plasma which can discharge the dielectrics and hold them near the mainframe potential.

### Summary and Conclusions

The electron emitter on ATS-5 was operated over one hundred times over a 4-yr period. These operations succeeded in reducing the magnitude of the potentials on the satellite, but rarely discharged the spacecraft completely. Transient negative potentials of greater size than the eclipse equilibrium value were seen when the neutralizer was switched off. Modeling of the current balance to the spacecraft showed that less than 1% of the emitted current was escaping the spacecraft at equilibrium. Three-dimensional modeling of the potentials and currents with NASCAP showed the development of differential potentials on the order of 100 V to be developed on the spacecraft surfaces, limiting the emission of the filament. This limitation was sufficient to explain the equilibrium potentials seen and would apply to most spacecraft with insulating surfaces. The NASCAP computer code was shown to be an effective tool in the modeling of three-dimensional charging problems, providing both the model of the limitation mechanism and the model for the time development of the observed effect. Laboratory modeling of the current limiting process provided similar results.

Experiments with a more powerful electron source, on the SCATHA satellite, produced results which were qualitatively similar to the ATS-5 results. Electron emission initially causes the satellite potential to rise toward zero, but limiting processes prevent the full electron beam from escaping and the satellite does not discharge. Ion beam emission experiments on ATS-5 showed no such difficulty at current levels comparable to the emitted photocurrent.

Operation of the ATS-6 engines and plasma bridge neutralizer had major effects on the spacecraft potential with respect to the ambient plasma as well as on the differential potentials on the spacecraft surface. The neutralizer or the engine could discharge large negative potentials at all times. Differential charging was reduced by the neutralizer when operated in spot mode, i.e., as an ion source, and eliminated by operation of the ion engine.

When the neutralizer was used in daylight cases of negative charging, i.e., in active environments, the neutralizer caused the spacecraft to rise to a few volts negative potential and reduced differential charging on the insulating surfaces of the spacecraft. Operation of the thruster in active environments

held the spacecraft at  $-4$  to  $-5$  V potential and eliminated the problem of differential charging. Fluxes of ions were seen from the engine and neutralizer when the spacecraft was in active environments.

The ATS-6 ion engine operations analyzed here show that plasma emission can be used to control spacecraft charging and does not generate differential potentials as electron emission does. A plasma source designed to control charging on a geosynchronous satellite needs to provide a sufficient current of thermal ions to hold shadowed dielectrics near the mainframe potential and a sufficient current of electrons to hold the mainframe near 0 V in eclipse. Plasma bridge design has not generally concentrated on optimization as an ion source but it appears that even the standard design used for ATS-6 or SERT 2 is adequate.<sup>20-22</sup> In the ATS-6 data set it appears that 1 mA is adequate to control the spacecraft potential. The bias of the plasma source will determine the potential of the spacecraft within certain limits. If the source is driven negative with respect to the spacecraft in an attempt to drive the spacecraft positive, the electron current drawn from the source to the spacecraft grows excessive. Biasing the source a few volts positive with respect to the spacecraft, as in the case of ATS-6, seems to be optimum for maintaining an ion current out toward the dielectrics surfaces. Development of plasma sources for potential control needs to be concentrated in the area of optimizing the plasma bridge or a similar device as an ion source with constraints of fuel and power usage. Concerns about ion contamination are probably best addressed by using a noble gas (xenon or argon) as a fuel.

### Acknowledgments

The particle data used herein were obtained from Dr. C.E. McIlwain of the University of California at San Diego. The ion engine experiment was the project of Dr. Robert Hunter and Mr. Robert Bartlett of NASA/GSFC, who also provided a great deal of help in the analysis of the data. Dr. Ray Goldstein of NASA/JPL also placed an important role in the analysis of the ATS-5 engine operations. Dr. Carolyn K. Purvis ran the ATS-5/NASCAP time-dependent computer model. This work was supported by NASA/LeRC under NSG-3150, with data acquired under NASA/GSFC Contract NAS 5-23481. Further support was provided by NASA/MSFC under NAS8-33982.

### References

- <sup>1</sup>DeForest, S.E., "Spacecraft Charging at Synchronous Orbit," *Journal of Geophysical Research*, Vol. 77, 1972, p. 651.
- <sup>2</sup>DeForest, S.E., "Electrostatic Potentials Developed by ATS-5," *Photon and Particle Interaction with Surfaces in Space*, edited by R.J.L. Grard, D. Reidel, Holland, 1973, pp. 263-276.
- <sup>3</sup>Reasoner, D.L., Lennartsson, W., and Chappell, C.R., "Relationship Between ATS-6 Spacecraft-Charging Occurrences and Warm Plasma Encounters," *Spacecraft Charging by Magnetospheric Plasmas*, Progress in Astronautics and Aeronautics Series, Vol. 47, edited by A. Rosen, AIAA, New York, 1976, pp. 89-102.
- <sup>4</sup>McPherson, D.A. and Schober, W.R., "Spacecraft Charging at High Altitudes," *Spacecraft Charging by Magnetospheric Plasmas*, Progress in Astronautics and Aeronautics Series, Vol. 47, edited by A. Rosen, 1976, pp. 15-30.
- <sup>5</sup>Whipple Jr., E.C., "Observations of Photoelectrons and Secondary Electrons Reflected from a Potential Barrier in the Vicinity of ATS-6," *Journal of Geophysical Research*, Vol. 81, 1976, p. 715-719.
- <sup>6</sup>Olsen, R.C., McIlwain, C.E., and Whipple, E.C., "Observations of Differential Charging Effects on ATS-6," *Journal of Geophysical Research*, Vol. 86, 1981, pp. 6809-6819.
- <sup>7</sup>Mauk, B.H. and McIlwain, C.E., "ATS-6 UCSD Auroral Particles Experiment," *IEEE Transactions on Aerospace and Electronic Systems*, Vol. AES-11, 1975, pp. 1125-1130.
- <sup>8</sup>Worlock, R.M., James, E.L., Hunter, R.E., and Bartlett, R.O., "ATS-6 Cesium Bombardment Engine North-South Stationkeeping Experiment," *IEEE Transactions on Aerospace and Electronic Systems*, Vol. AES-11, 1975, pp. 1176-1184.

<sup>9</sup>Goldstein, R. and DeForest, S.E., "Active Control of Spacecraft Potentials at Geosynchronous Orbit," *Spacecraft Charging by Magnetospheric Plasmas*, Progress in Astronautics and Aeronautics Series, Vol. 47, edited by A. Rosen, AIAA, New York, 1976, pp. 169-181.

<sup>10</sup>Olsen, R.C., "Modification of Spacecraft Potentials by Thermal Electron Emission on ATS-5," *Journal of Spacecraft and Rockets*, Vol. 18, Nov.-Dec. 1981, pp. 527-532.

<sup>11</sup>Whipple Jr., E.C., "The Equilibrium Potential of a Body in the Upper Atmosphere and in Interplanetary Space," NASA TN X-615-65-296, 1965.

<sup>12</sup>Katz, I. et al., "A Three Dimensional Dynamic Study of Electrostatic Charging in Materials," NASA CR 135256, 1977.

<sup>13</sup>Mandell, M.J., Katz, I., Schnuelle, G.W., Steen, P.G., and Roche, J.C., "The Decrease in Effective Photocurrents due to Saddle Points in Electrostatic Potentials near Differentially Charged Spacecraft," *IEEE Transactions on Nuclear Science*, Vol. 6, Vol. NS-25, 1978, p. 1313.

<sup>14</sup>Goldstein, R., "Active Control of Potential of the Geosynchronous Satellites ATS-5 and ATS-6," *Proceedings of the Spacecraft Charging Technology Conference*, edited by C.P. Pike and R.R. Lovell, NASA TMX-73537, AFGL-TR-77-0051, 1977, pp. 121-129.

<sup>15</sup>Gussenhoven, M.S. and Mullen, E.G., "Geosynchronous Environment for Severe Spacecraft Charging," *Journal of Spacecraft and Rockets*, Vol. 20, Jan.-Feb. 1983, pp. 26-34.

<sup>16</sup>Olsen, R.C., "Modification of Spacecraft Potentials by Plasma Emission," *Journal of Spacecraft and Rockets*, Vol. 18, Sept.-Oct. 1981, pp. 462-469.

<sup>17</sup>Grard, R.J.L., "Properties of the Satellite Photoelectron Sheath Derived from Photoemission Laboratory Measurements," *Journal of Geophysical Research*, Vol. 78, 1973, pp. 2885-2906.

<sup>18</sup>Olsen, R.C., "Field-Aligned Ion Streams in the Earth's Midnight Region," *Journal of Geophysical Research*, Vol. 87, 1982, pp. 2301-2310.

<sup>19</sup>Komatsu, G.K. and Sellen Jr., J.M., "A Plasma Bridge Neutralizer for the Neutralization of Differentially Charged Surfaces," *Effect of the Ionosphere on Space and Terrestrial Systems*, edited by J. Goodman, U.S. GPO, Washington, D.C., 1978, pp. 317-321.

<sup>20</sup>Kerslake, W.R., Goldman, R.G., and Neiberding, W.C., "SERT II: Mission Thruster Performance and In-Flight Thrust Measurement," *Journal of Spacecraft and Rockets*, Vol. 8, March 1971, pp. 213-224.

<sup>21</sup>Rawling, V.K. and Pawlik, E.V., "A Mercury Plasma-Bridge Neutralizer," *Journal of Spacecraft and Rockets*, Vol. 5, July 1968, pp. 814-820.

<sup>22</sup>Ward, J.W. and King, H.J., "Mercury Hollow Cathode Plasma Bridge Neutralizers," *Journal of Spacecraft and Rockets*, Vol. 5, Oct. 1968, pp. 1161-1164.

## *From the AIAA Progress in Astronautics and Aeronautics Series*

# SPACECRAFT RADIATIVE TRANSFER AND TEMPERATURE CONTROL—v. 83

*Edited by T.E. Horton, The University of Mississippi*

Thermophysics denotes a blend of the classical engineering sciences of heat transfer, fluid mechanics, materials, and electromagnetic theory with the microphysical sciences of solid state, physical optics, and atomic and molecular dynamics. This volume is devoted to the science and technology of spacecraft thermal control, and as such it is dominated by the topic of radiative transfer. The thermal performance of a system in space depends upon the radiative interaction between external surfaces and the external environment (space, exhaust plumes, the sun) and upon the management of energy exchange between components within the spacecraft environment. An interesting future complexity in such an exchange is represented by the recent development of the Space Shuttle and its planned use in constructing large structures (extended platforms) in space. Unlike today's enclosed-type spacecraft, these large structures will consist of open-type lattice networks involving large numbers of thermally interacting elements. These new systems will present the thermophysicist with new problems in terms of materials, their thermophysical properties, their radiative surface characteristics, questions of gradual radiative surface changes, etc. However, the greatest challenge may well lie in the area of information processing. The design and optimization of such complex systems will call not only for basic knowledge in thermophysics, but also for the effective and innovative use of computers. The papers in this volume are devoted to the topics that underlie such present and future systems.

*Published in 1982, 529 pp., 6×9, illus., \$35.00 Mem., \$55.00 List*

TO ORDER WRITE: Publications Dept., AIAA, 1633 Broadway, New York, N.Y. 10019